Meteorologische Zeitschrift, Vol. 23, No. 1, 33–49 (published online April 4, 2014)

What determines the differences found in forest edge flow between physical models and atmospheric measurements? – An LES study

Farah Kanani[1]*, Katja Träumner[2], Bodo Ruck[3] and Siegfried Raasch[1]

[1]Institute for Meteorology and Climatology, Gottfried-Wilhelm-Leibniz Universität Hannover, Germany
[2]Institute for Meteorology and Climate Research, Karlsruhe Institute of Technology, Germany
[3]Institute for Hydrodynamics, Karlsruhe Institute of Technology, Germany

(Manuscript received October 28, 2013; in revised form February 4, 2014; accepted February 11, 2014)

Abstract

A recent study has shown that Doppler lidar is a state-of-the-art method to obtain spatially and temporally resolved flow fields in forest edge flow regimes. In that study, the general flow features observed by lidar were found to be similar to those detected above a physical tree model in a wind tunnel. But in pivotal details, for example regarding the absolute height and the inner structure of the internal boundary layer (IBL), significant differences were detected. The main objectives of this Large-Eddy Simulation (LES) study are to analyze these differences and to associate them to the meteorological and physical differences between the set-ups of the wind tunnel and the atmospheric measurement. This enables on the one hand a model evaluation for the LES and the physical model respectively, and on the other hand a better understanding of the results from the lidar measurements. Results from an LES with neutral stratification and without Coriolis force show a similar IBL structure as in the wind tunnel and represent well-known characteristics of forest edge flow. A variation of the forest density only marginally affects the IBL structure. The presence of a finite forest clearing as observed at the lidar site increases the turbulence level of the IBL, compared to a set-up with a quasi-infinite clearing like in the wind tunnel. Including Coriolis force further enhances the turbulence levels to values observed by lidar. An increasing thermal instability results in even higher turbulence levels. Hence, differences between wind tunnel and atmospheric measurements are mainly traced back to differences in the flow forcing and in the onflow conditions upstream of the forest edge. Furthermore, a statistical analysis reveals that insufficient averaging of the lidar data also contributes to the observed deviations from the wind tunnel results. Based on this analysis, we suggest that at least two and a half hours of measurements during equivalent atmospheric conditions are necessary to obtain a statistically representative mean IBL structure.

Keywords: large-eddy simulation, forest edge flow, wind tunnel, doppler lidar, internal boundary layer

1 Introduction

Forest edges represent one of the most distinct discontinuities in natural surface conditions, leading to the development of complex turbulent flow structures. Due to form and viscous drag from trunks, branches and leaves the turbulent flow is significantly disturbed downstream of a forest edge. The mean flow is decelerated in front of and inside the forest, while a flow acceleration can be observed above the forest (e.g. Dupont and Brunet, 2009; Morse et al., 2002; Yang et al., 2006a), resulting from the narrowing of the flow cross-section. This produces a pronounced shear layer near the forest top with an inflection point in the vertical profile of mean streamwise velocity (e.g. Finnigan, 2000). As a result, Kelvin-Helmholtz instabilities are introduced to the flow and lead to the development of complex coherent turbulence structures (CTS) downstream of the forest edge (Dupont and Brunet, 2009). Starting from the edge, these CTS continuously grow in size and strength, until the flow properties have fully adjusted to the change in surface conditions (Belcher et al., 2012; Dupont and Brunet, 2009). Fully developed CTS scale with forest height (e.g. Finnigan, 2000; Finnigan et al., 2009; Raupach et al., 1996). They are strong enough to penetrate deep into the forest and therefore effectively contribute to the forest-atmosphere exchange of energy, momentum and trace gases such as CO_2 (e.g. Bergström and Högström, 1989; Finnigan, 1979; Katul et al., 1997; Raupach, 1981; Wallace et al., 1972). The layer above the forest, in which the flow adjustment takes place, is termed internal boundary layer (IBL). The IBL has been first studied in the context of abrupt changes in surface roughness (e.g. Garratt, 1990; Jegede and Foken, 1999). Above the IBL, the abruptly changing surface conditions have no effect on the turbulent flow.

Our present knowledge about forest edge flow has been drawn from a combination of field measurements, laboratory studies and numerical simulations. *In situ* tower measurements have been performed upstream

*Corresponding author: Farah Kanani, Institute for Meteorology and Climatology, Gottfried-Wilhelm-Leibniz Universität Hannover, Herrenhäuser Straße 2, Hannover 30419, Germany, e-mail: kanani@muk.uni-hannover.de

DOI 10.1127/0941-2948/2014/0542
Gebrüder Borntraeger Science Publishers, Stuttgart, www.borntraeger-cramer.com

and downstream of, within and above forests (e.g. Irvine et al., 1997; Kruijt et al., 1995; Raynor, 1971; Thomas et al., 2006; Zhu et al., 2004) to determine characteristic wind and momentum flux profiles for these regions and to understand the flow adjustment in transition flows. However, even though these tower measurements of e.g. turbulent CO_2 or heat fluxes are performed in the real world and therefore should truly represent the local atmospheric properties, the interpretation of these flux measurements is difficult. This is because the turbulent transport is highly variable within a forest-edge flow regime, spatially due to the surface transition and temporally due to variations of atmospheric conditions (e.g. Shaw et al., 1988). With wind tunnel (WT) studies of forest flow (e.g. Marshall et al., 2002; Morse et al., 2002; Ruck and Adams, 1991), multi-dimensional information on the turbulent wind field above the forest can be captured at lower costs compared to a set of tower measurements. However, due to the constraints of a WT, it is difficult to account for thermal stratification and to reproduce a typical atmospheric-boundary-layer wind profile. Moreover, it is rather difficult to measure the wind field inside the model forest with the available measuring techniques like e.g. particle image velocimetry.

Numerical simulation techniques like Large-Eddy Simulation (LES) have the advantage of being able to mimic atmospheric-boundary-layer features like the Ekman spiral and thermal stratification (e.g. Raasch and Franke, 2011; Steinfeld et al., 2007; Sühring and Raasch, 2013). Furthermore, LES can provide highly resolved information on the turbulent wind field in a forest-edge flow regime, even inside the forest (e.g. Bohrer et al., 2009; Cassiani et al., 2008; Dupont and Brunet, 2009; Schröttle and Dörnbrack, 2013; Yang et al., 2006a; Yang et al., 2006b). Atmospheric and plant physical conditions like wind speed, forest density and especially the thermal stability can be varied stepwise, at a much lower effort compared to a WT study. This way, the effect of each factor on e.g. the IBL structure can be systematically investigated.

But before LES can be reliably used for these applications, LES model results have to be validated against field measurements. Previous LES studies of forest edge flow (e.g. Yang et al., 2006a) have been tested against WT models and results from tower measurements, where the former cannot fully represent the atmospheric conditions and the latter cannot provide a complete multi-dimensional picture of the IBL structure. Thus, a validation of LES set-ups against field measurements that can provide a multi-dimensional view of the IBL structure above a forest is urgently needed. Recent studies by Träumner et al. (2012) revealed that Doppler lidar is a promising tool for this challenge. The lidar technique presents a state-of-the-art method to effectively complement *in situ* tower measurements near forest edges. Also Patton et al. (2011) have previously implemented Doppler lidar for coherent structure detection above an orchard within the CHATS (**C**anopy **H**orizontal **A**rray **T**urbulence **S**tudy) experiment.

Once validated, LES is besides a useful tool for virtually testing different lidar measuring strategies prior to an atmospheric measurement. LES data can be employed to investigate how e.g. the limited spatial resolution and the inherent averaging of the lidar or the limited temporal resolution due to the nature of the scan patterns affect the quality of the lidar measurement. With this approach lidar scan patterns can be optimized for appropriately capturing atmospheric flow phenomena like e.g. wind gusts or CTS above a forest. Stawiarski et al. (2013) showed first applications of this straight-forward approach.

In order to study the applicability of the lidar system for capturing turbulence structures above a forest, Träumner et al. (2012) compared streamwise velocity and corresponding standard deviation fields from atmospheric lidar measurements (AM) with those from laser Doppler anemometry measurements in the WT. The WT model was built to adequately represent the lidar measuring site (for details see Träumner et al., 2012). Lidar data were available for a number of stable and unstable cases, whereas the WT was operated under neutral conditions. Träumner et al. (2012) found a qualitative agreement between AM and WT data. The IBL height and the range of standard deviation above the WT forest were in between the observed values of the stable and the unstable cases of the AM. Too few neutral situations were detected in the AM data for a direct comparison with the neutral situation in the WT. Despite this general agreement, no quantitative agreement regarding a visually estimated IBL height and concerning the values of the normalized standard deviation could be found. The unstable cases in the AM showed a faster IBL growth and higher standard deviations. This deviation from the WT data might be explained by the differences in atmospheric stability and flow forcing, being a distinct difference between AM and WT. Another difference lies in the characteristics of the approaching flow. At the lidar site, a forest patch and houses were present approximately 1.5 km upstream of the examined clearing-to-forest transition, while the approaching WT flow was not disturbed by any upstream forest patch. This might create different onflow conditions, because the flow reaching the lidar forest edge can still be affected by the upstream located obstacles when the clearing length turns out to be insufficient. Moreover, there might have been deviations in forest structure and density between the real and the modeled forest, since exact information about these quantities were not available for the lidar site. The efficiency of the flow distortion by a forest increases with increasing forest density (e.g. Cassiani et al., 2008). These mentioned uncertainties concern the ability of remodeling the AM conditions in the WT. Regarding the AM dataset, insufficient statistics might have also caused a deviation from the WT data.

Using LES, one objective of the present study is to identify which of the above mentioned uncertain-

ties can explain the observed differences between AM and WT. For this purpose different LES set-ups are simulated to investigate the effect of forest density, clearing length, Coriolis force and atmospheric stability on the IBL structure. LES especially enables to examine the effect of atmospheric stability, which is one of the main differences between the WT set-up and the AM conditions. Furthermore, it is investigated if the available lidar statistics allow to identify the mean IBL structure, which would be representative for the conditions during the sampling periods of the AM data. Another objective of this LES study is to reproduce the distinct IBL deformation that was observed in the AM data. This step provides the opportunity of testing our LES model and the used set-ups against multi-dimensional data from the field. It shall be noted that the present investigation focuses on situations with moderately strong wind speeds and does not refer to the simulation of individual severe wind gusts, which have been investigated e.g. in a recent wind tunnel study by Tischmacher and Ruck (2013).

Prior to the discussion of the results, a brief description of the field experiment, wind tunnel model and LES set-ups is given in the following chapter. As a first step of the systematic parameter study, the LES data of an idealized WT-like set-up with neutral stratification are compared to the WT data. The discussion of these results is presented together with the results of the parameter studies in the third chapter of this article, followed by a summary of the conclusions.

2 Measurement and model set-up

2.1 Doppler Lidar experiment

Doppler lidars use pulses of infrared light to remotely determine the line-of-sight velocity of aerosol particles in the atmosphere, which move with the wind. Depending on the used pulse width, the pulse repetition frequency and the sampling frequency, the line-of-sight wind can be measured with a spatial resolution of 10 to 100 m and a precision of approximately 0.15 m s^{-1}.

In a field study in winter 2009/2010 two Doppler lidars, a passive temperature and humidity profiler as well as an energy balance station were set-up near a forest edge in Hatzenbühl (Germany) to investigate the wind field in front of and above the forest (Träumner et al., 2012). The used lidar data for the present study were obtained by the Doppler lidar "WindTracer" (from Lockheed Martin Coherent Technologies Inc.) in a scanning mode, moving the laser beam in vertical slices perpendicular to the forest edge from 0 to 10 ° elevation. Details of the instrument can be found in Träumner et al. (2011).

The lidar data were divided by the cosine of the elevation angle to estimate the horizontal wind velocity, projected on a Cartesian grid with a horizontal resolution of 50 m, and a vertical resolution of 15 m and averaged over 15 min. For the following discussion of the results, a 15-min average is defined as one ensemble member (EM). For a wind direction nearly perpendicular to the edge, 28 EM with stable and nine EM with unstable atmospheric conditions were available. This resulted in one ensemble average over the stable cases and one ensemble average over the unstable cases. Since heat flux data were not available for all of the selected EM, the classification into stable and unstable EM was based on vertical temperature gradients (stable: $\frac{\partial\theta}{\partial z} > 0.001\,\mathrm{K\,m^{-1}}$, unstable: $\frac{\partial\theta}{\partial z} < -0.001\,\mathrm{K\,m^{-1}}$), derived from vertical profiles of the potential temperature in the lowest 300 m. Overall, heat fluxes covered a range of $-0.03\,\mathrm{K\,m\,s^{-1}}$ to $0.05\,\mathrm{K\,m\,s^{-1}}$ during this measuring campaign.

Differently to the WT and the LES, the flow direction cannot be kept constant and perpendicular during the AM and might show natural variations. However, the EM from the lidar measurements were chosen in a way that it is reasonable to assume that the mean velocity component perpendicular to the line-of-sight is zero.

The used set-up and analysis technique enables a two-dimensional vertical view of the wind field from about 850 m in front of the forest edge to 1000 m behind the edge, with a vertical extension of 75 m closest to the lidar and up to 850 m downstream of the edge. Upstream of the forest edge, another forest patch and a residential area were present, starting at a distance of $\sim$ 1.5 km from the edge.

2.2 Wind tunnel model

A tree model of the forest at the Hatzenbühl site was constructed with a scale of 1:200 and positioned in a closed 29-m long atmospheric boundary layer wind tunnel. An initial wind profile following a power law with a profile exponent of 0.26 was applied. The wind velocity in front of and above the model forest was measured with a two-dimensional laser Doppler anemometer along sixteen vertical profiles at heights of 0 to 0.4 m (0 to 80 m) at locations from 0.1 m (20 m) in front of the edge to 1.3 m (260 m) in the tree stand. A detailed description of this technique can be found in (Ruck, 1987). For more information on the WT set-up see also Träumner et al. (2012).

2.3 Large-Eddy Simulation

2.3.1 Model basics

For the presented study, the **PA**rallelized **L**ES **M**odel PALM[1] (Raasch and Etling, 1998; Raasch and Schröter, 2001) was used for a dry atmosphere. PALM is based on the non-hydrostatic incompressible Boussinesq equations and the conservation equations of energy and mass. Advection terms were solved according to the fifth-order scheme after Wicker and Skamarock (2002). A third-order Runge-Kutta scheme was

[1] At revision 874, http://palm.muk.uni-hannover.de/browser?rev=874

applied for the time integration (Williamson, 1980). The Poisson equation for pressure that ensures incompressibility, was solved by the means of Fast Fourier Transformation. To model the effect of turbulence scales smaller than the numerical grid size on the large-scale flow (Deardorff, 1980), an additional prognostic equation is solved for the subgrid-scale (SGS) turbulent kinetic energy (TKE). Random perturbations were initially imposed on the horizontal velocity field to trigger turbulence. Lateral domain boundaries were cyclic. No-slip conditions were prescribed at the domain surface and the surface momentum fluxes were parametrized using Monin-Obukhov Similarity Theory (Monin and Obukhov, 1954). At the upper domain boundary, free-slip conditions were applied.

PALM has been successfully used to simulate various atmospheric and laboratory scenarios under neutrally (e.g. Letzel et al., 2008) and weakly stably stratified conditions (Steinfeld et al., 2007), as well as under convective conditions (e.g. Raasch and Franke, 2011). Flow phenomena have not only been investigated above homogeneous surfaces, but also within heterogeneously heated convective boundary layers (e.g. Letzel and Raasch, 2003; Steinfeld et al., 2008; Sühring and Raasch, 2013) and in neutrally stratified flows around obstacles (Inagaki et al., 2012).

The effect of the forest on the turbulent flow was modeled by a canopy model, which is implemented in PALM according to Shaw and Schumann (1992) and Watanabe (2004). Due to form (pressure) and viscous drag, the forest acts as a sink for momentum. This behavior is described at each numerical grid point as a grid-box-averaged effect on the resolved-scale turbulent flow by adding the term $F_{u_i} = c_\mathrm{d}\, a\, U\, \overline{u}_i$ to the momentum equations:

$$\frac{\partial \overline{u}_i}{\partial t} = -\frac{\partial\left(\overline{u}_k\,\overline{u}_i\right)}{\partial x_k} - \frac{\partial \overline{p}}{\partial x_i} - \frac{\partial \overline{p^*}}{\partial x_i} + \frac{\overline{\theta^*}}{\theta_0}\, g\,\delta_{i3} - \frac{\partial \tau_{ki}}{\partial x_k} - F_{u_i}\,. \tag{2.1}$$

An overbar denotes the spatial filtering of the subgrid scales, which corresponds to a volume (grid box) average. Indices $i,k \in \{1,2,3\}$ describe edge-perpendicular, edge-parallel and vertical velocity components $u_1 = u$, $u_2 = v$, $u_3 = w$ and spatial coordinates $x_1 = x$, $x_2 = y$ and $x_3 = z$, respectively. Remaining quantities are time t, kinematic pressure p, perturbation pressure p^*, potential temperature fluctuation θ^* from the horizontal mean, reference state θ_0, gravitational acceleration g, and the Kronecker delta δ. Implying K-theory, the SGS stress tensor $\tau_{ki} = -K_\mathrm{m}\left(\frac{\partial \overline{u}_i}{\partial x_k} + \frac{\partial \overline{u}_k}{\partial x_i}\right)$, with $K_\mathrm{m} = c_\mathrm{m}\, l\, \sqrt{e}$ being the turbulent diffusion coefficient for momentum. The Smagorinsky coefficient c_m is set to 0.1 and e is the SGS TKE, which is calculated by an additional prognostic equation as described further below. The mixing length l under neutral and unstable conditions equals either the numerical grid length Δ or 1.8 times the distance to the surface, whichever is the smaller value. The efficiency of momentum reduction by the forest canopy as described in term F_{u_i} depends on drag coefficient c_d, leaf area density a, absolute velocity $U = (\overline{u}^2 + \overline{v}^2 + \overline{w}^2)^{1/2}$ and the respective velocity component $\overline{u}_i$. Furthermore, the forest also has an effect on the unresolved small-scale turbulence, which is considered by the additional term $F_e = 2\, c_\mathrm{d}\, a\, U\, e$ in the prognostic equation for the SGS TKE e:

$$\frac{\partial e}{\partial t} = -\frac{\partial\left(\overline{u}_k\, e\right)}{\partial x_k} - \tau_{ki}\frac{\partial \overline{u}_i}{\partial x_k} + \frac{g}{\theta_0}\, W_3 + \frac{\partial}{\partial x_k}\left(2\, K_\mathrm{m}\frac{\partial e}{\partial x_k}\right) - \epsilon - F_e\,, \tag{2.2}$$

with W_3 being the vertical component of the SGS sensible heatflux $W_k = -K_\mathrm{h}\,\frac{\partial \overline{\theta}}{\partial x_k}$, where θ is the potential temperature and $K_\mathrm{h} = K_\mathrm{m}\left(1 + \frac{2l}{\Delta}\right)$ is the turbulent diffusion coefficient for heat. The dissipation rate ϵ is parametrized by $\epsilon = \left(0.19 + 0.74\,\frac{l}{\Delta}\right)\frac{e^{3/2}}{l}$.

With the widely used approach for F_e, proposed by Shaw and Schumann (1992), it is assumed that plant elements rapidly break down turbulence structures to smaller scales. It is further assumed that this small-scale turbulence, generated as wake turbulence in the lee of plant elements, is smaller than the energy-containing scales of SGS TKE and therefore rapidly dissipated (Edburg et al., 2012). This type of canopy model has been successfully applied in LES studies of homogeneous canopy flow (e.g. Kanda and Hino, 1994; Shaw and Schumann, 1992; Su et al., 1998; Su et al., 2000; Watanabe, 2004) as well as forest edge flow (e.g. Cassiani et al., 2008; Dupont and Brunet, 2008, 2009; Yang et al., 2006a; Yang et al., 2006b).

When simulating a heated atmospheric boundary layer, the forest additionally acts as a source $F_\theta = \frac{\partial Q_\theta}{\partial z}$ for heat (Shaw and Schumann, 1992) in the first law of thermodynamics:

$$\frac{\partial \overline{\theta}}{\partial t} = -\frac{\partial\left(\overline{u}_k\,\overline{\theta}\right)}{\partial x_k} - \frac{\partial W_k}{\partial x_k} - F_\theta, \tag{2.3}$$

F_θ is described as the vertical derivative of the upward vertical kinematic heat flux

$$Q_\theta(z) = Q_\theta(H)\exp(-\alpha P),\; P = \int_z^H a\, dz\,. \tag{2.4}$$

$Q_\theta(H)$ is the prescribed heat flux at the forest top ($z = H$), starting of which the heat fluxes at the different levels inside the forest are calculated by this decaying exponential function of the downward cumulative plant area index P. The extinction coefficient α is set to 0.6. With this approach it is assumed that the foliage inside the forest is heated by the solar radiation penetrating into the forest, according to the distribution of net radiation as suggested by Brown and Covey (1966). This parametrization has been applied in LES of canopy flow by Shaw and Schumann (1992) as well as Bohrer

et al. (2009), and found independently in high resolution LES with resolved tree canopy structures by SCHRÖTTLE and DÖRNBRACK (2013).

The set of model equations is completed by the continuity equation for an incompressible flow: $\frac{\partial \overline{u}_k}{\partial x_k} = 0$.

2.3.2 Simulation set-ups

Prior to the comparison between lidar and LES data, PALM and the applied canopy model were tested against the WT data. The flow across an idealized forest edge was simulated under neutral conditions, representing the situation in the WT as closely as possible. The model domain extended over $154\,H \times 38\,H \times 13\,H$ in streamwise (x), spanwise (y) and vertical (z) direction, with $H = 30\,\mathrm{m}$ being the forest height (Fig. 1). A grid resolution of 3 m was used in each direction, resolving the forest with 10 grid points in the vertical. In a sensitivity study with different grid sizes (not shown), this resolution has been tested to be sufficient to resolve the canopy-scale turbulence structures. The forest covered $33\,H$ (= forest length L_{Fo}) of the domain length L_{x} and extended over the total domain width L_{y}. With the cyclic boundary conditions, this resulted in a total clearing length of $L_{\mathrm{Cl}} = L_{\mathrm{x}} - L_{\mathrm{Fo}} = 121\,H$. The domain height was chosen in a way that developing CTS are not affected by the free-slip rigid domain top. With the chosen domain width, being a multiple of the separation scale of CTS (e.g. FINNIGAN et al., 2009), it was assured that the CTS are properly captured. The forest was assumed to be horizontally homogeneous. This is in slight contradiction to the real forest and the WT set-up, where the individual tree heights and species (broad-leafed trees, conifers) were considered. However, the vertical structure was inhomogeneous as described by the vertical profile of plant area density a in Fig. 2, where the vertical axis has been normalized with forest height H. The plant area index $\mathrm{PAI} = \int_0^H a(z)\,dz$ was set to 8 for this first simulation, hereafter named **PAI8**, and varied to 2 and 4 in the following studies. The value of PAI = 8 lies within the typical range of forest densities observed in coniferous and broad-leafed forests, as present at the lidar site. A constant canopy drag coefficient of $c_{\mathrm{d}} = 0.2$ was assumed, which is a typical value for trees and has been applied in other forest-edge-flow studies (e.g. CASSIANI et al., 2008; DUPONT and BRUNET, 2008; KATUL and ALBERTSON, 1998). In accordance to the WT conditions, the Coriolis force was neglected. The flow forcing was accomplished by a constant direct pressure gradient of $\frac{\partial \overline{p}}{\partial x} = -0.0017\,\mathrm{Pa\,m^{-1}}$ (see third term of Eq. 2.1) in the x-direction, assuring for a purely edge-perpendicular flow at all heights. This value was determined by tuning the pressure gradient in order to match the mean wind profiles of LES and WT (Fig. 3). For normalization, the values $u_{\mathrm{ref}} = 8.3\,\mathrm{m\,s^{-1}}$ in the LES and $u_{\mathrm{ref}} = 7.6\,\mathrm{m\,s^{-1}}$ in the WT were taken at the forest edge at $2\,H$ above the ground. A constant roughness length of $z_0 = 0.1\,\mathrm{m}$ was set for the forested as well as for the non-forested area. Since the forest acts as the main momentum sink, this value does not really come into effect for the forested surface and is just prescribed for completeness.

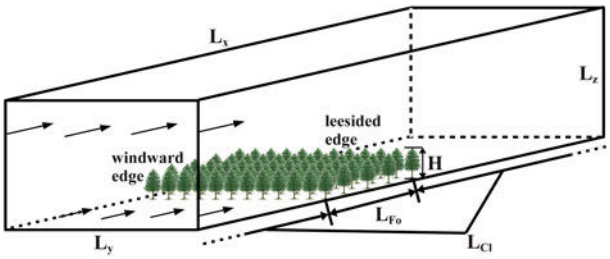

Figure 1: Sketch of the LES model domain. L_{x}, L_{y}, L_{z} are domain length, width and height, respectively. The forest extends over a length of L_{Fo} in x-direction and over the total domain width L_{y}. The forest height is $H = 30\,\mathrm{m}$. The clearing length $L_{\mathrm{Cl}} = L_{\mathrm{x}} - L_{\mathrm{Fo}}$ describes the total length of the unforested part of the domain. The forest edge is oriented perpendicular to the mean flow (marked by arrows).

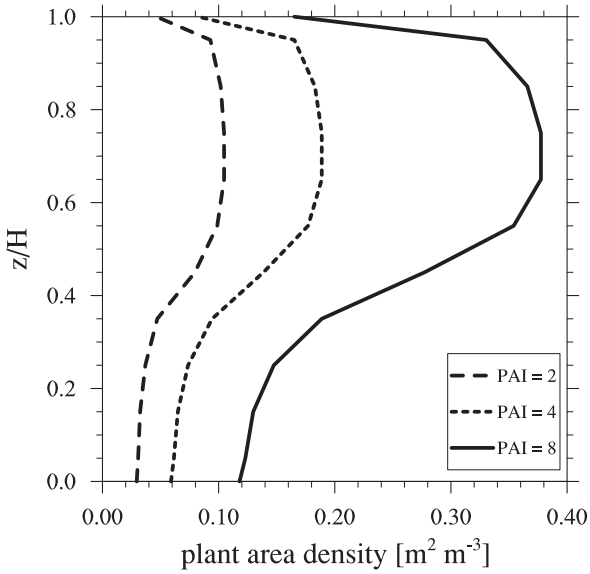

Figure 2: Vertical profiles of different plant area densities. The ordinate is normalized with forest height H. Plant area indices (PAI) of 2, 4 and 8 are used, each with the same vertical plant distribution.

In the following, the set-ups of the parameter studies are described and summarized in Tab. 1. As information on forest density of the real and the model forest was not available, **PAI8** was repeated with PAI = 2 (**PAI2**) and PAI = 4 (**PAI4**) to quantify the effect of forest density on the IBL structure, c.f. Fig. 2 in DUPONT and BRUNET (2009). Thereby the vertical distribution of plant area was maintained (Fig. 2). One difference between the lidar experiment and the WT set-up were the different onflow conditions. While a forest patch and houses were present 1.5 km upstream of the examined forest edge at the lidar site, the flow across the WT forest was not disturbed by any upstream forest edge. In order to study the effect of an upstream located forest on the IBL development downstream of a clearing-to-forest transition, LES with different clearing lengths L_{Cl} were conducted. The existence of an upstream located forest

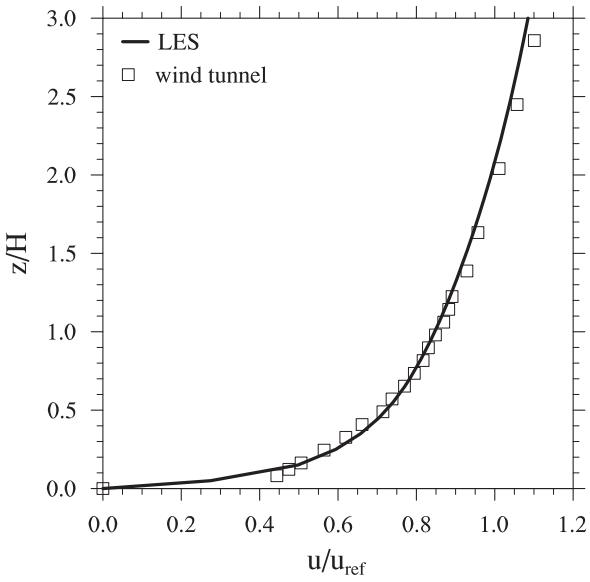

Figure 3: Vertical profiles of u-velocity (edge-perpendicular component) from wind tunnel (squares) and LES (solid line). Profiles are taken at $x = -1H$ ($1H$ upstream of the windward edge) and are normalized with reference speed $u_{\mathrm{ref}} = u(x = 0H, z = 2H)$. The ordinate is normalized with forest height H. Velocities are time averaged and LES data are additionally averaged along the edge-parallel direction.

Table 1: Overview of the used LES set-ups (N: neutral, U: unstable, Q: prescribed kinematic heat flux at clearing surface and forest top).

LES run	PAI	L_{cl}	Coriolis force	stratification	u_{ref} ($\mathrm{m\,s^{-1}}$)
PAI8	8	$121\,H$	no	N	8.3
PAI2	2	$121\,H$	no	N	8.5
PAI4	4	$121\,H$	no	N	8.3
LCL5	8	$51\,H$	no	N	8.4
LCL10	8	$102\,H$	no	N	9.6
LCL20	8	$204\,H$	no	N	10.7
GEO-N	8	$51\,H$	yes	N	5.3
GEO-U1	8	$51\,H$	yes	U ($\mathrm{Q = 0.05\,K\,m\,s^{-1}}$)	6.4
GEO-U2	8	$51\,H$	yes	U ($\mathrm{Q = 0.1\,K\,m\,s^{-1}}$)	7.0

edge in the LES results from the cyclic lateral boundary conditions. Based on the set-up of **PAI8**, clearing lengths of $L_{\mathrm{Cl}} = 51H$, $L_{\mathrm{Cl}} = 102H$ and $L_{\mathrm{Cl}} = 204H$ (**LCL5**, **LCL10** and **LCL20**) were simulated. The aspect ratio $r = L_{\mathrm{Fo}} / L_{\mathrm{Cl}}$ was held constant at 0.5 among the three simulations to keep the averaged surface friction in the model domain constant. This setting is necessary to maintain the shape of the vertical profile of the mean wind, so that the flow conditions of the three simulations are as similar as possible.

Another difference between lidar experiment and WT set-up was that Coriolis force and thermal stratification could not be considered in the latter. In order to quantify the effect of these differences in atmospheric conditions on the IBL structure, LES with geostrophic forcing were conducted under **N**eutral (**GEO-N**) and **U**nstable (**GEO-U**) conditions, based on the set-up of **LCL5** where the clearing length matches the one at the lidar site. Under atmospheric conditions, the pressure term in Eq. 2.1 is described by $\frac{\partial \overline{p}}{\partial x_i} = \varepsilon_{ijk} f_j \overline{u}_k + \varepsilon_{i3k} f_3 \overline{u}_{k_{\mathrm{g}}}$. Index g denotes the geostrophic wind components u_{g} and v_{g}, which were set to $10.0\,\mathrm{m\,s^{-1}}$ and $-4.5\,\mathrm{m\,s^{-1}}$ respectively. The Coriolis parameter $f_i = (0, 2\,\Omega\cos(\varphi), 2\,\Omega\sin(\varphi))$ is described by the Earth's rotation $\Omega = 2\pi/24\,\mathrm{hr}$ and the chosen latitude $\varphi = 55^\circ$. With the wind shift with height due to the Coriolis force, this forcing produces a near-surface flow direction approximately perpendicular to the forest edge. The domain height was increased to 2700 m, in order to allow the Ekman-layer wind profile to develop appropriately. To save computational resources, the vertical grid spacing was gradually stretched to 25 m above $z = 450\,\mathrm{m}$, which is well above the levels affected by the forest edge. The simulations with unstable stratification (**GEO-U**) were additionally driven by a constant sensible heat flux, with the same value at the clearing surface and the forest top. By keeping the heat input homogeneous, the IBL development can be studied purely as a result of roughness changes, with additional effects of buoyancy. Two simulations were conducted with heat fluxes of $0.05\,\mathrm{K\,m\,s^{-1}}$ (**GEO-U1**) and $0.1\,\mathrm{K\,m\,s^{-1}}$ (**GEO-U2**). These values were chosen to provide a general estimate about the behavior of the IBL development for moderately and strongly heated atmospheric boundary layers. There was no attempt to simulate the real heat fluxes, because flux values were not available for the sampling period of the unstable lidar EM. Both simulations were initialized with a constant $\theta = 300\,\mathrm{K}$ up to $z = 500\,\mathrm{m}$, followed by a strong inversion of $0.01\,\mathrm{K\,m^{-1}}$ up to the domain top. For a better comparability of these atmospheric LES with results from field measurements or other LES, some background information is presented. Figure 4 presents Hovmöller diagrams of the horizontally and half-hourly averaged $\theta(z/H, t)$ for the LES cases **GEO-U1** (a) and **GEO-U2** (b). In both cases, the well-mixed convective boundary layer warms due to the prescribed surface heating, which leads to an increase of the boundary-layer depth z_{i} in the temporal evolution. Thereby z_{i} is defined as the height at which the vertical temperature gradient reaches its maximum value (following Sullivan et al., 1998). As expected, θ and in turn z_{i} increase faster when a stronger surface heating is present (**GEO-U2**). The average z_{i} (over last three hours) equals $34\,H$ ($\widehat{=}\,1020\,\mathrm{m}$) for **GEO-U1** and $40\,H$ ($\widehat{=}\,1200\,\mathrm{m}$) for **GEO-U2**. We calculated vertical profiles of the Richardson number $Ri = \frac{g/\theta_0\,\partial\theta/\partial z}{(\partial u_{\mathrm{h}}/\partial z)^2}$, derived from the horizontally and temporally averaged vertical profiles of θ and $u_{\mathrm{h}} = \sqrt{u^2 + v^2}$. For the two convective regimes **GEO-U1** and **GEO-U2**, maximum Ri values of -1.5 and -4.0 were found respectively within the convective boundary layer.

The overbar in Eq. 2.1–2.3 is not carried along after this point.

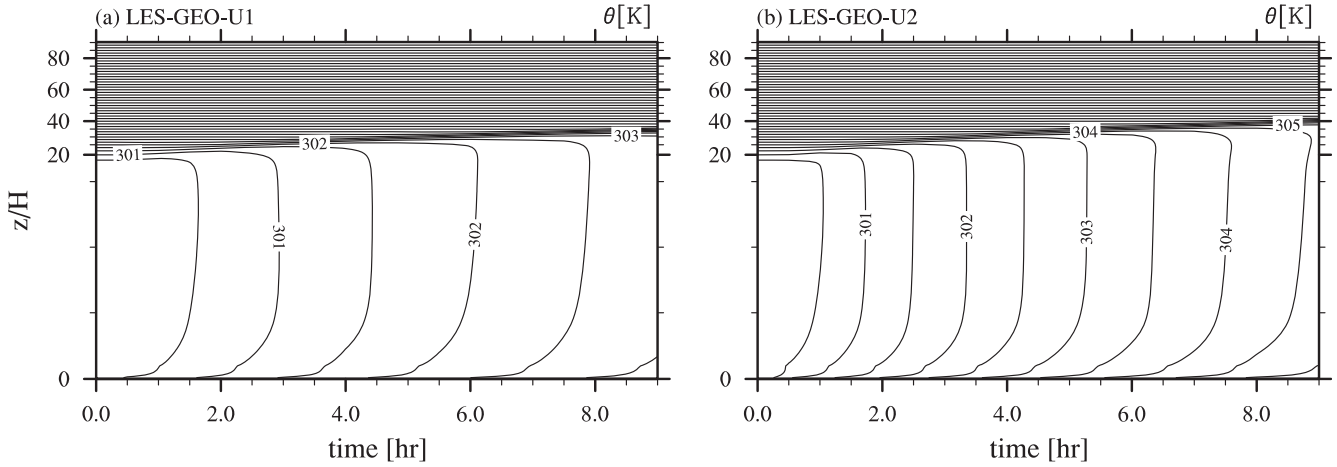

Figure 4: Hovmöller diagrams of the horizontally and half-hourly averaged potential temperature θ for the LES cases (a) **GEO-U1** and (b) **GEO-U2**.

2.3.3 Analysis Methods

The comparison between LES, AM and WT data was based on streamwise vertical slices of standard deviation σ_u of streamwise velocity u. This quantity was used exclusively, as it was also used as a basis for the comparison between the AM and WT data in Träumner et al. (2012), and it provides information about the turbulence level and is therefore adequate to retrieve information about the IBL structure. σ_u was calculated in the same way as for AM and WT datasets, using the temporal eddy-covariance method (e.g. Foken, 2008).

The vertical slices of σ_u were output after the flow had reached a (quasi-) stationary state. To exclude the effect of different mean background wind speeds between AM, WT and the different LES, resulting from the different atmospheric conditions, all presented data were normalized with an individual reference velocity u_{ref} of the respective AM, WT and LES cases. In the LES data, the calculation of σ_u was based on a three-hour time average of the u-velocity, and for better statistics, the calculated σ_u was hereafter averaged along the edge-parallel direction, if not mentioned otherwise.

To evaluate the effect of the parameters on the IBL structure, the IBL heights were calculated for each presented dataset. Several approaches exist to estimate the IBL depth, summarized by Garratt (1990). The IBL top in the present study is defined at the height above which $\sigma_u \leq 1.01\sigma_{u_0}$ (following Shir, 1972). According to Shir (1972), who used the surface stress to estimate the IBL depth related to a pure roughness change, σ_{u_0} is the near-surface value of σ_u upstream of the forest edge, where flow characteristics should be representative for the underlying surface conditions. However, with σ_{u_0} values taken from certain distances upstream of the forest edge, calculated IBL heights deviated up to $1\,H$ from visually identified IBL heights. The reason for this difference is that with a relatively short clearing length of $51\,H$, used in several simulations to match lidar site conditions, the flow above the clearing has not fully adjusted to the surface conditions after having been disturbed at the leesided forest edge. Thus, the flow reaching the windward forest edge still carries the turbulence that has been produced above the forest upstream of the clearing. Therefore, these σ_{u_0} values are not representative for the surface conditions of the clearing. To take into account that the advected turbulence increases the turbulence level in front of and above the forest, a modified σ_{u_0} was calculated by averaging σ_u values at $x = -1\,H$ within a layer between $z = 2\,H$ and $z = 3\,H$. This specific layer average of σ_{u_0} was used because it represented the only overlap between AM, WT and LES data at this specific x-position.

To quantify which fraction of the observed difference in turbulence level between AM and WT can be attributed to each parameter, an IBL-averaged σ_u ($\langle\sigma_u\rangle_{IBL}$) was calculated. For comparison reasons, $\langle\sigma_u\rangle_{IBL}$ was defined in all datasets as the average over the IBL region from $z = 1.4\,H$ to the IBL top and up to a distance of $10\,H$ downstream of the forest edge, because this was the maximum coverage of the WT data.

Furthermore, the shear length scale $L_s = \frac{u(H)}{(\partial u/\partial z)_{z=H}}$ (Raupach et al., 1996) that defines the depth of the shear layer at the canopy top, was calculated for a better comparability of our results with results from previous LES studies and field experiments.

3 Results and discussion

To illustrate the IBL development behind a forest edge, a snapshot[2] of the absolute value of the three-dimensional rotation $|\zeta| = |\varepsilon_{ijk}\,\partial_{x_j} u_k|$ is presented in Fig. 5. The snapshot is taken after three hours of simulation time from LES **PAI8**. This quantity has been chosen for this

[2]The corresponding animation is available under http://palm.muk.uni-hannover.de/wiki/gallery/movies/forest. It was created with VAPOR, a product of the Computational Information Systems Laboratory at the National Center for Atmospheric Research, www.vapor.ucar.edu

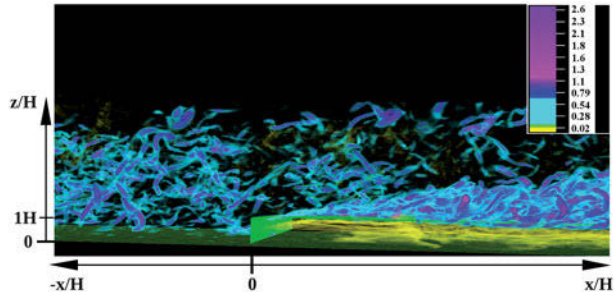

Figure 5: Three-dimensional snapshot of the absolute value of the three-dimensional rotation $|\zeta| = |\varepsilon_{ijk}\,\partial_{x_j} u_k|$ [s^{-1}] after three hours of simulation time from **PAI8**. High values in pink illustrate strong turbulence, lower values in yellow mark areas with weak turbulence. The mean flow is directed from left to right and the forest edge is oriented perpendicular to the streamwise direction. The forest edge is at $x = 0\,H$ and is marked by the light green isosurface.

illustration as it is a measure for the flows turbulence intensity. The mean flow direction is from left to right and the forest edge is at $x = 0\,H$, marked by the green isosurface. High rotation values are drawn in pink, low values in yellow and intermediate values in blue.

Figure 5 illustrates to what extent a turbulent flow is modified when coming up against a forest edge. In front of the forest, the approaching flow is rather turbulent, with different scales of turbulence being quite unorganized. Entering the forest, the turbulence is damped due to pressure and viscous drag forces. Meanwhile above the forest, turbulence is effectively generated due to the strong velocity shear near the forest top. With increasing distance from the forest edge, the developing turbulence structures grow in size and strength, forming a layer of high turbulence activity, within the flow adjusts to the new surface conditions. This layer represents the IBL.

3.1 Comparison between LES and wind tunnel data

As a first step, the LES data of **PAI8** are compared to the WT data. This step is taken to demonstrate the capability of PALM, with the implemented canopy model, to adequately reproduce the IBL properties downstream of a forest edge. Figure 6 presents normalized standard deviation σ_u/u_{ref} from WT (a) and LES (b). Axes are normalized with forest height H and the forest edge is located at $x = 0\,H$. White space in the plots masks areas where WT or AM data are not available due to technical constraints. LES data are available inside the forest, but to keep the focus on the area of interest above the forest, this area is masked in the LES data as well. The dashed black lines represent the IBL tops, calculated as described in Sect. 2.3.3.

Data of WT and LES generally show a qualitative and quantitative agreement regarding the shape of the IBL and the turbulence intensity. As expected, the IBL grows with distance to the forest edge, resulting from the nature of the CTS evolution of e.g. horse shoe vortices as simulated for forest canopy flow by Finnigan et al. (2009). The maximum values of σ_u do not occur directly behind the edge but further downstream. This behavior corresponds to previous findings (e.g. Dupont and Brunet, 2008; Morse et al., 2002) and can also be explained by the stepwise development process of CTS behind forest edges. As previously explained, the developing CTS grow in size and strength with increasing distance to the edge and thus, the strongest CTS occur further downstream from the edge. Additionally, the turbulence production is suppressed in the region near the forest edge, where the mean upward-directed flow, as a result from horizontal flow deceleration, transports relatively slow and less turbulent air out of the forest (e.g. Dupont and Brunet, 2008; Morse et al., 2002). Regarding the observed turbulence level from WT and LES, similar σ_u values have been reported by Yang et al. (2006a), derived from field, WT and numerical experiments. The overall agreement between WT and LES data allows the conclusion that our simulations adequately account for the drag effect of the forest on the turbulent flow. Our LES model can therefore be used to expose the reasons for the differences found between real-world lidar measurement and wind tunnel study.

3.2 Comparison between LES and field data

On the right-hand side of Fig. 6, the corresponding AM data are presented for the unstable (c) and the stable (d) ensemble averaged cases. The dashed black lines again mark the IBL tops. For the stable case (d), the 1 % σ_u-criterion had to be changed to 35 % to determine a reasonable IBL top, because under stable conditions the relatively small upstream σ_u values are not retained anywhere above the forest (as can be seen in Fig. 7 (b)). The relatively small σ_u values below $z = 3\,H$ in front of the forest edge can be attributed to the fact that the stable thermal stratification is most pronounced near the surface. Hence, turbulence suppression is much stronger there than in larger heights or above the forest.

Comparing Fig. 6 (c) and (d) with the neutral LES case (b), it is evident that IBL height and range of σ_u values of the neutral LES lie in between the lidar observations under unstable and stable conditions, as also observed by Träumner et al. (2012) for the comparison between AM and WT data. In the unstable case, the IBL grows faster and higher than under neutral or stable conditions, probably caused by the additional turbulence generation by buoyancy, what will be discussed in Sect. 3.3.3. In turn, the suppression of turbulence under stable conditions leads to the observed lower IBL height and σ_u values. Now the question arises, whether the differences between AM and WT data can be purely explained by the effect of different stratification. Comparing e.g. the $\langle\sigma_u\rangle_{IBL}$ values of the unstable lidar case (c) and the WT (a) with $0.23\,u_{ref}$ and $0.19\,u_{ref}$, respectively, results in a deviation of nearly 20 %. Besides the stratification, the effect of Coriolis force or differences in plant physical conditions such as forest density and clearing length might also be relevant and are therefore investigated in the following.

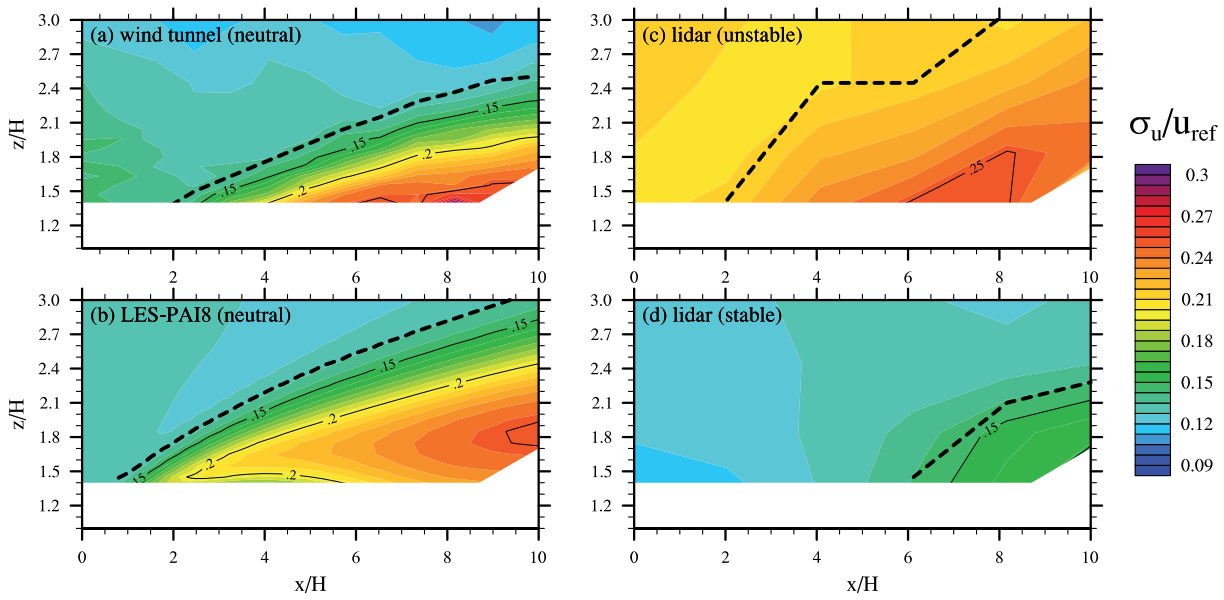

Figure 6: Streamwise vertical slices of mean normalized standard deviation σ_u/u_{ref} from (a) wind tunnel and (b) LES **PAI8** under neutral conditions and from the lidar measurements under (c) unstable and (d) stable conditions. The dashed black lines mark the IBL tops. Isolines are plotted at steps of 0.05. Axes are normalized with forest height H and the forest edge is at $x = 0H$. White space masks areas where wind tunnel and lidar data are not available. For a better comparison, this area is also masked in the LES plot, even though LES data are available within the forest.

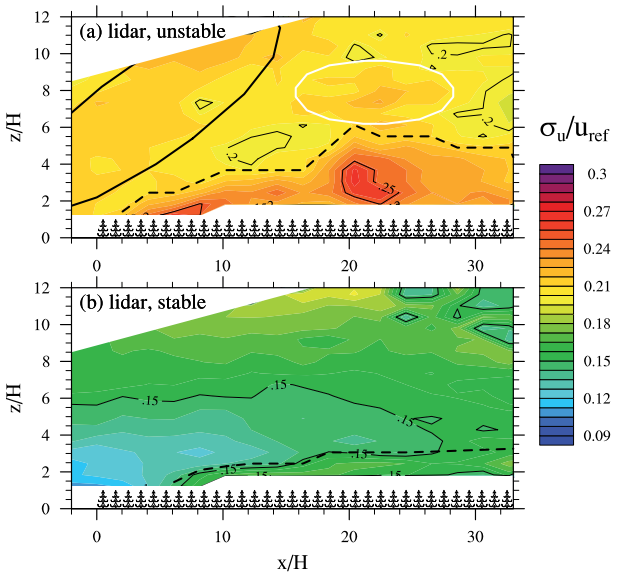

Figure 7: Lidar observations for (a) unstable and (b) stable conditions, as in Fig. 6 (c,d), but for an extended region. Trees mark the canopy layer. The white circle highlights an area with relatively high σ_u values, which might or might not be attributed to the IBL. The occurence of such large structures in the σ_u field makes a clear identification of the IBL height difficult.

Since the lidar observations are the starting point for this investigation, the σ_u-slices of Fig. 6 (c) and (d) are presented for a horizontally and vertically extended region in Fig. 7 (a) and (b), respectively. Providing two-dimensional flow information for such an elongated area in the field is a unique feature of the Doppler lidar measurements. Looking at the extended σ_u-field in Fig. 7 (a) first of all reveals that a clear identification of the IBL height is difficult. The IBL as bounded by the dashed black line has no smooth boundary. Moreover, it is not clear whether or not the large region of enhanced turbulence (white circle) is to be attributed to the IBL, which would significantly modify the IBL structure. According to the applied IBL criterion, the white-circled area does not belong to the IBL. However, the same high σ_u values that are observed within the IBL also occur within the circled area, which somehow connects this area to the IBL. The most probable reason for this indefinite IBL structure in the unstable lidar case is that the ensemble average over the available nine EM is insufficient to average out larger-scale turbulence structures, which occur in the form of convection or strong wind gusts. In order to try to reproduce the occurrence of such larger structures in the LES data, a statistical analysis was additionally carried out. This analysis will be presented subsequent to the discussion of the parameter study.

3.3 Effects of plant physical and atmospheric parameters on IBL development

3.3.1 Forest density

As forest density information of the real forest was not available, the effect of an incorrectly modeled forest density on the IBL structure was investigated. Results for plant area indices of 2, 4 and 8 (**PAI2**, **PAI4**, **PAI8**) are presented in Fig. 8 (a–c), showing mean normalized standard deviation σ_u/u_{ref} for the same region as in Fig. 7. The dashed black lines mark the calculated IBL tops. In contrast to AM and WT data, LES data are

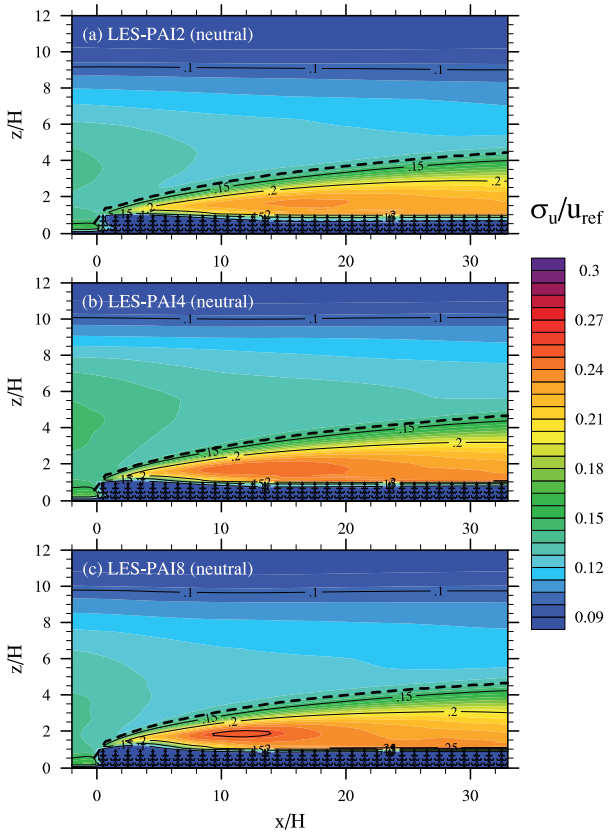

Figure 8: Streamwise vertical slices of mean normalized standard deviation σ_u/u_{ref} from LES under neutral stratification with different forest densities: (a) **PAI2**, (b) **PAI4** and (c) **PAI8**. The same region as in Fig. 7 is plotted. Trees mark the canopy layer. Dashed black lines mark the IBL tops. For comparison reasons, isolines are additionally plotted at steps of 0.05.

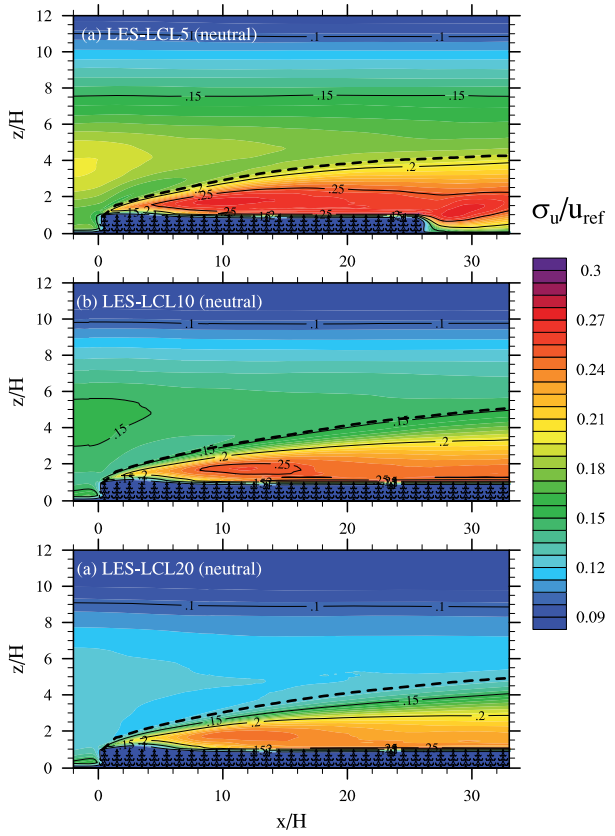

Figure 9: Same as Fig. 8 (c) with PAI = 8, but with different clearing lengths: (a) $L_{Cl} = 51H$ (**LCL5**), (b) $L_{Cl} = 102H$ (**LCL10**) and (c) $L_{Cl} = 204H$ (**LCL20**). The forest lengths L_{Fo} differ between the three cases, because the aspect ratio $r = L_{Fo}L_{Cl}^{-1}$ was held constant at 0.5. For that reason, the forest in (a) already ends at $x \approx 26H$.

also available inside and right above the forest, but these regions are not subject of the present investigation.

The comparison of **PAI2** (a), **PAI4** (b) and **PAI8** (c) shows no significant effect of forest density on IBL height. However, with a denser canopy, higher values of σ_u occur within the IBL, indicating that stronger CTS develop above denser forests. For example, the maximum σ_u value of $0.25\,u_{ref}$ for **PAI8** is 5 % higher than the value for **PAI2**. At the same time, the maximum σ_u values can be found closer to the forest edge. These findings for σ_u can also be detected for the vertical momentum fluxes (not shown; calculated analogous to σ_u respective the variance of u). One exception is that the IBL height is slightly lower for all **PAI** cases by about $0.4H$ compared to the IBL heights derived from σ_u. And overall, the IBL momentum fluxes (absolute values) are smaller than σ_u^2 by a factor of four, which agrees well with findings by Finnigan (2000) and Yang et al. (2006a).

Regarding the adjustment of the momentum fluxes for different PAI, similar findings were reported by Dupont and Brunet (2009), i.e. that momentum fluxes are higher above denser forests and the maximum fluxes occur closer to the forest edge. They attributed this behavior to the development of the different CTS stages, which they found to be faster above denser canopies. This results from the stronger wind shear above denser forests (not shown), which forms due to the stronger flow deceleration within and acceleration above the canopy, caused by the higher drag. The stronger shear in turn leads to stronger turbulence generation and hence to a faster flow adjustment. The adjusted shear lengths of $L_s/H = 0.37$ (**PAI2**), $L_s/H = 0.25$ (**PAI4**) and $L_s/H = 0.17$ (**PAI8**) also agree well with those determined by Dupont and Brunet (2009) as presented in their Fig. 4. Our L_s values further blend in nicely with data from wind tunnel and field experiments, as summarized by Raupach et al. (1996) and later also discussed by Finnigan (2000), lending further confidence to our results.

However, since different forest densities produce only slight differences in the IBL structure, an incorrectly modeled forest density is probably not responsible for the observed large differences between AM and WT data.

3.3.2 Clearing length

In order to study the effect of upstream located obstacles on the forest edge flow with respect to the difference between AM and WT conditions, simulations with

clearing lengths of $L_{Cl} = 51H$ (**LCL5**), $L_{Cl} = 102H$ (**LCL10**) and $L_{Cl} = 204H$ (**LCL20**) were carried out (Fig. 9 (a–c)), based on the set-up of **PAI8**. As mentioned earlier, the forest lengths L_{Fo} differ here, because the aspect ratio r was held constant to assure for a constant averaged surface friction.

Just like for the forest density, a variation in L_{Cl} exhibits no significant effect on the IBL height (marked by dashed black lines). It should be noted that the IBL heights are only similar up to $x \approx 20H$, because the forest in **LCL5** does not extend beyond $x = 26H$, in contrast to the other cases. In contrast to the similar IBL heights, the general level of σ_u values is found to increase with decreasing clearing length. For instance, $\langle\sigma_u\rangle_{IBL}$ is with a value of $0.24\,u_{ref}$ for **LCL5** 20 % higher than for **LCL20**. The maximum σ_u value of $0.29\,u_{ref}$ for **LCL5** is 12 % higher compared to the value for **LCL20**. These higher values result from the fact that for shorter clearings the level of the advected turbulence from the leesided edge is still higher when reaching the windward forest edge, which contributes to the total IBL turbulence level. For example the background turbulence level, quantified by σ_{u_0} (Sect. 2.3.3) increases from $0.16\,u_{ref}$ (**LCL20**) to $0.19\,u_{ref}$ (**LCL5**), i.e. by 16 %. The advection of a higher turbulence level, compared to the background turbulence above the IBL, can also be observed in the AM data (Fig. 7 (a): region between solid black lines). The higher turbulence level is advected from the upstream located houses and trees (not shown). Despite the increase in turbulence intensity from **LCL20** to **LCL5**, the adjusted shear lengths are equal for all **LCL** cases, with $L_s/H = 0.17$ near the far end of each forest. This indicates that L_s, i.e. the depth of the shear layer, seems to depend mainly on forest density (see Sect. 3.3.1) and not on the effect of upstream obstacles. And this further confirms that the modification of the IBL structure from **LCL20** to **LCL5** is mainly a result of the modified background turbulence rather than of a modified shear layer.

Overall, higher σ_u values should be expected with shorter clearings. Hence, the presence of the upstream located forest patch and houses at the lidar site, which were not considered in the WT, can produce significantly higher turbulence levels. However, $\sigma_{u_0} = 0.19\,u_{ref}$ in **LCL5** is still 10 % lower than $\sigma_{u_0} = 0.21\,u_{ref}$ in the unstable lidar case. The large differences in IBL height between AM and WT data cannot be explained by the effect of the clearing length.

3.3.3 Atmospheric stability

Contrary to the WT and the so far discussed LES set-ups, the lidar experiment took place in a real atmospheric boundary layer, where the atmospheric stability is usually never strictly neutral and where depending on the stability a more or less pronounced Ekman layer describes the boundary-layer wind profile. To estimate the effect of the background wind profile and the atmospheric stability on the IBL structure, additional LES

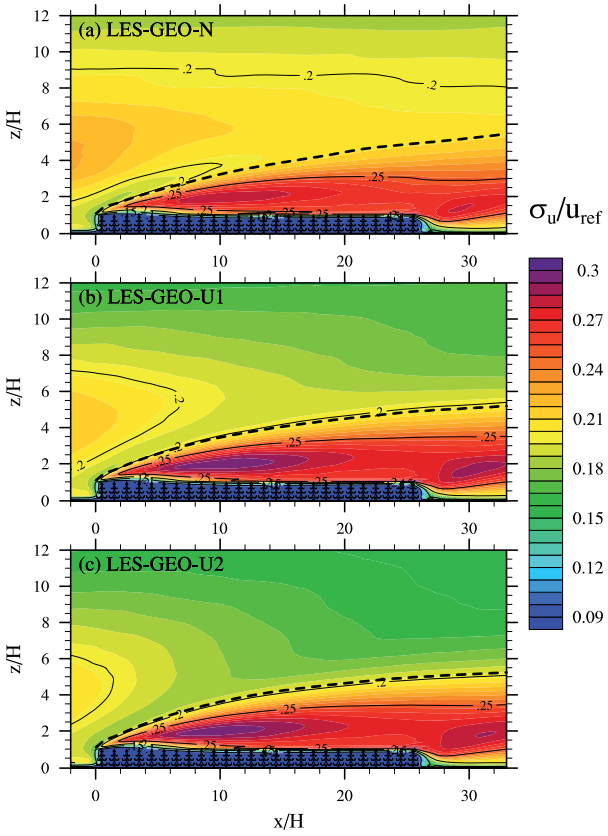

Figure 10: Same as Fig. 9 (a), but with a geostrophic flow forcing under (a) neutral conditions (**GEO-N**) and unstable conditions with kinematic heat fluxes of (b) $0.05\,K\,m\,s^{-1}$ (**GEO-U1**) and (c) $0.1\,K\,m\,s^{-1}$ (**GEO-U2**), prescribed homogeneously at the clearing surface and the forest top.

with geostrophic forcing under neutral and unstable conditions were conducted. These simulations were based on **LCL5**, as the clearing length of this case matches the one at the lidar site and the IBL turbulence level agreed already well with the level in the unstable lidar case.

Switching from direct pressure gradient forcing (**LCL5** in Fig. 9 (a)) to geostrophic forcing (**GEO-N** in Fig. 10 (a)) slightly modifies the IBL height. The IBL in the latter case grows slightly faster so that at $x = 20H$ it is about $1H$ higher than in the former case. This can be attributed to the stronger shear in **GEO-N**, due to the additional directional shear, that allows the developing CTS to propagate further upward than in **LCL5**. Another difference to **LCL5** is the overall higher IBL turbulence level in **GEO-N**, which is with $\langle\sigma_u\rangle_{IBL} = 0.25\,u_{ref}$ an increase of 4 %. The higher σ_u values are directly connected to the higher turbulence level of the background flow, which is advected from the leesided forest edge, as already reported in the previous section. Although the same clearing length is used in both cases, the advected turbulence level (σ_{u_0}) that reaches the windward edge is higher in **GEO-N** by 10 %. The reason for this is again the stronger shear, which helps to maintain the higher turbulence level over a longer distance from the lee edge.

Now with a characteristic atmospheric background wind profile (with Coriolis force), not only the IBL properties but also the background turbulence levels closely match those observed by lidar under unstable stratification (Fig. 7 (a)). While σ_{u_0} deviates by 35 % between the WT and the unstable lidar case, the σ_{u_0} values of the latter case and **GEO-N** are nearly equal with both being approximately $0.21\,u_{ref}$. This finding allows the conclusion that the effect of a freely developing atmospheric wind profile versus a WT profile can additionally cause significant quantitative discrepancies regarding the level of turbulence, as observed by Träumner et al. (2012) between AM and WT data.

Under unstable conditions (**GEO-U1**), controlled in the LES by homogeneous surface and forest-top heating, the turbulence level in the lower part of the IBL slightly increases (Fig. 10 (b)) compared to the neutral case **GEO-N** (a). The maximum σ_u values of $0.28\,u_{ref}$ for **GEO-N** and $0.29\,u_{ref}$ for **GEO-U1** deviate by about 3 %. This can be associated with the effect of buoyancy that supports the CTS development due to the additional thermal instability. A similar finding was reported by Bohrer et al. (2009), who determined based on field and LES data that buoyancy contributes to or takes over part of the TKE production above the forest. They further stated that the TKE production by convection is characterized by a larger integral length scale, which might explain the slightly faster growth of the IBL from **GEO-N** to **GEO-U1**. But nevertheless, the IBL reaches the same height of $z = 4.75H$ at $x = 20H$ in both cases. Figure 10 (b) further reveals that the effect of the leesided edge is less pronounced under unstable conditions, i.e. lower turbulence levels are advected than in **GEO-N**. This results from the fact that the flow from the forest-to-clearing transition adjusts faster to the conditions above the clearing (not shown), what can be attributed to the large scale vertical mixing above the clearing due to the effect of buoyancy. Despite the homogeneous heating, the relative effect of buoyancy is much more pronounced above the clearing because the effect of shearing is relatively weak here. Above the forest, this relation is reversed, as most of the turbulence is generated by the strong wind shear. Now as can be seen in the upper part of the IBL, the σ_u values are smaller than in **GEO-N**, caused by the overall weaker background turbulence. This effect does not hold for the lower IBL part, where the buoyancy effect is more present. Overall, the mean IBL turbulence level increases by 4 % from **GEO-N** to **GEO-U1**. Increasing the heating from $0.05\,\mathrm{K\,m\,s^{-1}}$ (**GEO-U1**) to $0.1\,\mathrm{K\,m\,s^{-1}}$ (**GEO-U2**; Fig. 10 (c)) does not significantly modify the IBL properties. The effect of the leesided forest edge further decreases due to the further enhanced vertical mixing above the clearing, decreasing the turbulence level in the approaching flow. The IBL σ_u values remain nearly constant because the effect of the even weaker background turbulence compensates the effect of the stronger heating. We assume that the contribution of the shear-induced CTS to the IBL turbulence level is invariant here, as Thomas et al. (2006) found from tower measurements under varying atmospheric conditions that these CTS showed no dependency on atmospheric stability.

The above mentioned findings hold for the applied moderately strong wind speeds. At low wind speeds, the effect of buoyancy is suspected to dominate the effects of wind shear and therefore might prevent the development of an IBL, but this is yet to be investigated in detail. The highest σ_u values of **GEO-U1** and **GEO-U2** with nearly $0.3\,u_{ref}$ were not observed in the AM data (Fig. 7 (a)), although, with vertical temperature gradients in the range of -0.001 to $-0.004\,\mathrm{K\,m^{-1}}$, the thermal instability of the unstable lidar EM seemed to be similar to the one in **GEO-U1** ($\frac{\partial\theta}{\partial z} = -0.002\mathrm{K\,m^{-1}}$) and **GEO-U2** ($\frac{\partial\theta}{\partial z} = -0.004\mathrm{K\,m^{-1}}$). But since more concrete information on the thermal instability, e.g. based on measured heatfluxes, are not available for these lidar cases, we cannot make a definite statement at this point. Due to this incomplete information, our aim was not to reproduce the unstable lidar-experiment conditions, but rather to demonstrate possible effects of an unstable stratification on the IBL development for moderately and relatively strong heated atmospheric boundary layers.

The so far presented results show that variations of the parameters clearing length (i.e. upstream obstacles), Coriolis force and thermal instability (positive buoyancy) can cause deviations in the IBL turbulence level, which are of the same magnitude as the difference between the WT and the unstable lidar case. We can estimate that under (nearly) neutral conditions, an incorrect consideration of the clearing length or the total neglect of upstream obstacles has the major effect. Compared to the Coriolis-force effect on $\langle\sigma_u\rangle_{IBL}$ with 4 %, the consideration of a finite clearing as present at the lidar site produced a 20 % higher $\langle\sigma_u\rangle_{IBL}$. Hence, the latter has a five-fold stronger effect. Under unstable conditions, it is complicated to separately distinguish the relative importance of each parameter based on the available LES data. This is connected with the fact that e.g. in a convective boundary layer, the effect of the Coriolis force is less pronounced due to the well-mixed state of the boundary layer. Furthermore, it was found that the advection of turbulence from the upstream forest decreases from neutral to unstable conditions. But in order to explicitly quantify the remaining importance of the clearing length relative to the buoyancy effect, further LES studies under unstable conditions need to be conducted. The understanding of forest edge flow in such conditions is still rather limited. We assume though that especially for short clearings with $L_{Cl} < 50H$ and relatively weak thermal instabilities, the neglect of an upstream forest in the WT probably leads to significantly larger errors than the assumption of neutral conditions.

Up to this point, the investigated parameters are all related to the possibility on how far the conditions from the field can be reproduced in the WT. But as previously mentioned, a clear identification of the IBL char-

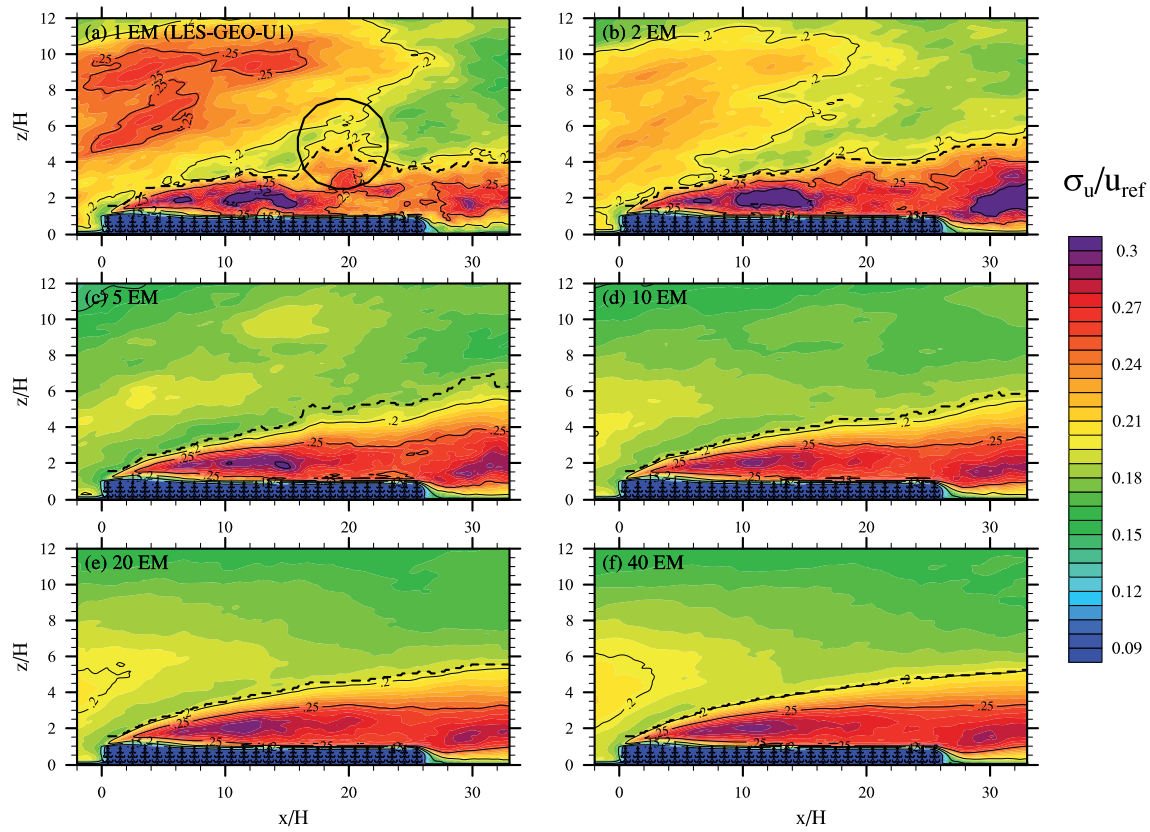

Figure 11: Same as Fig. 10 (b), but instead of the edge-parallel average an ensemble average over (a) one, (b) two, (c) five, (d) ten, (e) 20 and (f) 40 ensemble members was applied. Analogous to the lidar EM, one LES EM corresponds to a 15-min-average of a single vertical slice.

acteristics could not be drawn for the unstable lidar case (Fig. 7 (a)), as the occurrence of a large turbulence structure (white circle) substantially deformed the IBL. This deformation is possibly caused by a thermal vortex, as e.g. discussed by Thomas et al. (2006) for field measurements and by Schröttle and Dörnbrack (2013) for LES, but it might also be caused by strong intermittent wind gusts that are known to occur near forest edges (e.g. Dupont and Brunet, 2008, 2009; Yang et al., 2006a). In both cases, the IBL deformation indicates that statistics are insufficient to average out the effect of such individual flow structures on a statistically reliable mean IBL. Therefore, results of a statistical analysis are discussed in the following section.

3.4 Effect of insufficient statistics on the detection of the IBL structure

If the number of EM is not large enough to average out eventually occurring larger turbulence structures, turbulence statistics are insufficient to produce a well-defined mean state of the IBL, regarding the IBL height and the inner structure. This problem arises especially under unstable conditions, where generally larger structures occur than under stable conditions. For the former case, only nine lidar EM were available.

The following investigation of the statistics was therefore based on the unstable LES case **GEO-U1**. It shall be exemplarily demonstrated how far the mean IBL structure deviates, in case of insufficient averaging of e.g. thermal vortices, from the results of the 3-hr time- and line-averaged reference **GEO-U1** in Figure 10 (b), which is assumed to be the virtual reality. For this purpose, Fig. 11 presents ensemble averages over different numbers of EM: (a) 1 EM, (b) 2 EM, (c) 5 EM, (d) 10 EM, (e) 20 EM, (f) 40 EM. Analogous to one lidar EM, one LES EM thereby comprises a 15-min average of one individual (not line averaged) streamwise vertical slice of σ_u/u_{ref}. The individual LES EM are sampled from the last three hours of the simulation **GEO-U1**, spatially and temporally independent in a statistical sense. The spread in the flow conditions between the EM, e.g. in the quantity u_{ref}, is less than 5 % with an average $u_{ref} \approx 6.5\,\mathrm{m\,s^{-1}}$.

It is evident from Fig. 11 (a) that in case of only one EM (**GEO-U1-1EM**), the whole picture strongly deviates from the reference **GEO-U1** (10 (b)). For instance, the IBL boundary exhibits a distinct deformation (Fig. 11 (a), black circle), similar to the lidar observations (Fig. 7 (a), white circle), whereas the reference **GEO-U1** shows a smooth and continuous growth of the IBL. In addition, the maximum σ_u value for **GEO-U1-1EM** is nearly 13 % higher than for reference **GEO-U1**, and it occurs almost $5H$ further downstream. The relatively chaotic structure of the IBL in Fig. 11 (a) complicates e.g. an estimation of the different stages of the flow adjustment, which can be a valuable information

for the interpretation of tower measurements. A further large difference between **GEO-U1-1EM** and **GEO-U1** can be detected in the appearance of the advected background flow. The advected turbulence level within the high-turbulence plume bounded by the 0.2-isoline in **GEO-U1-1EM** takes maximum σ_u values of $0.26\,u_{ref}$, which is 20 % higher than the advected maximum values for **GEO-U1**. Moreover, this large-scale plume in **GEO-U1-1EM** reaches significantly larger heights and distances downstream of the windward forest edge as the advected turbulence in the reference **GEO-U1**. And this plume even partly connects with the IBL. Such a plume of relatively high σ_u values can also be observed in the lidar data (Fig. 7 (a)), in the area between the solid black lines.

The fact that this pronounced upward-directed plume vanishes in the LES with an increasing EM number (Fig. 11 (a–f)) indicates that the plume in the lidar data might indeed be an artifact of insufficient averaging. Also the IBL deformation in **GEO-U1-1EM** is smoothed out with an increasing number of EM, which is an additional indication that the IBL deformation in the lidar data might also be a result of an insufficient EM number. Overall, the different LES ensemble averages demonstrate that an increasing EM number has a smoothing effect on the IBL boundary and the inner IBL structure. Thereby, the IBL σ_u values converge towards the values of the reference **GEO-U1**. Looking e.g. at the relative difference between the $\sigma_u(x/H, z/H)$ in the IBL of **GEO-U1** and the $\sigma_u(x/H, z/H)$ in the corresponding region of each **GEO-U1-#EM** reveals that maximum differences decrease from 21 % (**GEO-U1-1EM**) to 10 % (**GEO-U1-10EM**) and finally reach 5 % for **GEO-U1-40EM**. The IBL averages of the differences decrease from 8 % (**GEO-U1-1EM**) to 5 % (**GEO-U1-10EM**) and take values of 2 % for both **GEO-U1-20EM** and **GEO-U1-40EM**. Thus, if the margin of the error by insufficient averaging is e.g. desired to be less than 5 %, we suggest to average over more than 10 EM with equal atmospheric conditions.

We are aware that atmospheric conditions are highly non-stationary, not only from day to day, but also or especially in the course of a day. Consequently, we propose that much more than 10 EM from a confined range of atmospheric conditions are necessary, to obtain a statistically relevant picture of the mean flow structure above a forest, which can be representative for this specific range of conditions (e.g. regarding wind speed and direction, atmospheric stability). Based on these findings we can conclude that the 9 lidar EM forming the unstable case, which were obtained from four different days with variations in u_{ref} between 2.7 and 7.0 m s^{-1}, variations in $\frac{\partial\theta}{\partial z}$ (in the lowest 300 m) between 0.001 and 0.004 K m^{-1} and Ri from -2 to -7, were not sufficient to fulfill this purpose. We further assume that in windy (nearly) neutral conditions, where buoyancy effects might be neglected, the number of required EM with equal atmospheric conditions can be less than ten. This assumption is based on the smaller integral time scale of now dominating shear-induced CTS with 20–30 s, compared to the time scale of attached thermal eddies with 190–210 s (e.g. Thomas et al., 2006). And according to Lenschow et al. (1994), flows with smaller integral time or length scales require smaller averaging periods for obtaining a certain measuring accuracy, as opposed to flows with larger length scales.

4 Summary

A recent study by Träumner et al. (2012) has identified Doppler lidar to be a state-of-the-art technique to obtain two-dimensional information of the turbulent flow field in forest edge flow regimes. While general flow features were found to be similar in comparison with laser Doppler anemometry data from a dedicated wind tunnel study, quantitative differences were detected regarding the absolute height and the inner structure of the IBL. Compared to the data from the neutrally stratified wind tunnel, IBL height and turbulence strength was found to be higher for the unstable lidar cases and lower for the stable lidar cases. This comparison by Träumner et al. (2012) was based on the standard deviation σ_u of streamwise velocity.

One main objective of this LES study was to analyze these differences and to associate them to the meteorological and physical differences between the set-ups of the wind tunnel and the atmospheric measurement. In the present investigation, several differences were identified between the set-ups, regarding thermal stratification, flow forcing, presence of obstacles upstream of the forest edge and forest density. In order to determine which of these parameters might be responsible for the detected deviations in the IBL properties, different LES parameter studies were conducted. As a first step, the IBL properties as observed in the wind tunnel data could be reproduced using a wind-tunnel-like LES set-up. Based on the parameter studies, the observed deviations between the atmospheric lidar measurement and the wind tunnel could mainly be traced back to differences in the onflow and the background flow conditions. The forest density showed only minor effects on IBL height and the detected turbulence levels.

The presence of upstream located obstacles (forest patch and houses upstream of the clearing-to-forest transition at the lidar site), which were not considered in the wind tunnel, was found to have the major effect on the IBL turbulence level. With decreasing clearing length (unforested region) in the LES, the IBL turbulence level increases to values found in the lidar data, which can be ascribed to the enhanced advection of turbulence produced above the upstream located forest patch. Hence, with the presence of upstream obstacles, turbulence levels are expected to be higher than with a quasi-infinite clearing like in the wind tunnel, especially for clearings shorter than 50 forest heights. The effect of the upstream forest patch was determined to be most pronounced under neutral conditions. Under unstable conditions, this

effect decreases with increasing instability due to the large scale vertical mixing by thermal plumes, which promotes the adjustment of the flow to the surface conditions of the clearing. Although not investigated within the scope of this study, it is presumed that the advection of turbulence from the leesided edge will also be less pronounced under conditions with a stable thermal stratification, where turbulence is damped due to the negative buoyancy.

Accounting for the effect of the Coriolis force and the thermal stratification on an atmospheric measurement, both of which cannot be reproduced in most wind tunnels, exposed to have a major effect on the background turbulence level. The Coriolis force increases the mean vertical shear of the flow in the neutral LES, which enhances the overall turbulence level compared to the LES without Coriolis force. But this increase is much more pronounced for the background turbulence than for the IBL turbulence, and it is in the same range as the increase in the background turbulence level when considering a finite rather than a quasi-infinite clearing. Regarding the IBL turbulence level, the clearing length was found to have a five-fold stronger effect than the Coriolis force. Under unstable conditions, the additional effect of positive buoyancy leads to a slight increase of the IBL turbulence level, which is of the same magnitude as the increase after consideration of the Coriolis force. These findings hold for the applied moderately strong wind speeds, where the above-canopy turbulence production by wind shear dominates the production by positive buoyancy. Situations where buoyancy significantly dominates over shear, e.g. with weak winds and strong convection, might not even at all permit the development of an IBL. A thorough investigation of the IBL structure downstream of a forest edge under various atmospheric stability and wind speed regimes is subject to further study. Of special interest should thereby be the interplay of the buoyancy effect on the relative effect of the clearing length, since our first results have indicated that the effect of the latter might be less pronounced under unstable than under neutral conditions.

The other objective of this LES study was to try to reproduce the distinct IBL deformation, which occurred in the data of the unstable lidar case and thus prevented a clear identification of the IBL. By using an atmospheric LES set-up with unstable thermal stratification, a likewise deformed IBL could be detected when statistics were insufficient to average out larger-scale turbulence structures like thermal eddies. On the one hand, this agreement with two-dimensional field data confirmed that our LES model is capable of appropriately modeling the turbulent flow above a forest canopy. On the other hand, the statistical analysis revealed that the available nine 15-min-averages from the lidar, where atmospheric conditions (wind speed, thermal instability) differed to some extent, were not sufficient to produce a mean state of the IBL, which can be representative for this range of observed conditions. It was shown with the LES that at least ten 15-min-averages, i.e. two and a half hours worth of data from equal atmospheric conditions are necessary to reduce the error in the IBL structure due to insufficient averaging to 5 %. Hence, much more than two and a half hours of data should be available for an atmospheric measurement, since the atmosphere is usually never strictly stationary, i.e. atmospheric conditions change on different time scales. The number of required 15-min-averages thereby depends on the covered range of atmospheric conditions and should be increased with increasing range. To summarize, with the help of LES we were able to identify reasons for the distinct differences observed by Träumner et al. (2012) between data from atmospheric measurements and from the wind tunnel.

Overall, Doppler lidar is a state-of-the-art tool to capture turbulence structures above forests as volume averages and, given that statistics are sufficient, to provide two-dimensional information of mean IBL characteristics. While lidar is the only way of providing these multi-dimensional information in the field, LES can be used for systematic parameter studies under realistic atmospheric conditions at a relatively low effort. To make use of these possibilities, LES results have to be validated against multi-dimensional field data, which can be supplied by lidar. In turn, LES is a helpful tool to a priori test the suitability of different Doppler lidar measuring strategies. We want to emphasize that a combined application of lidar and LES is essential to thoroughly investigate the IBL structure behind forest edges and the turbulent transport by CTS for various atmospheric regimes.

5 Acknowledgments

This work was supported by the German Research Foundation (DFG) under grant number [RA 617/23-1]. Special thanks to Andreas Wieser, who designed and implemented the measuring set-up and contributed valuable ideas to this project. All simulations were performed on the SGI Altix ICE at The North-German Supercomputing Alliance (HLRN) in Hannover and Berlin. NCL[3] and VAPOR[4] have been used for data analysis and visualization. We appreciate the two anonymous reviewers for their constructive and valuable comments that helped to improve this manuscript.

References

Belcher, S., I. Harman, J. Finnigan, 2012: The wind in the willows: flows in forest canopies in complex terrain. – Ann. Rev. Fluid Mech. **44**, 479–504.

Bergström, H., U. Högström, 1989: Turbulent exchange above a pine forest ii. organized structures. – Bound.-Layer Meteor. **49**, 231–263.

[3]The NCAR Command Language (Version 6.1.2) [Software]. (2013). Boulder, Colorado: UCAR/NCAR/CISL/VETS. http://dx.doi.org/10.5065/D6WD3XH5

[4]A product of the Computational Information Systems Laboratory at the National Center for Atmospheric Research, www.vapor.ucar.edu

Bohrer, G., G. Katul, R. Walko, R. Avissar, 2009: Exploring the effects of microscale structural heterogeneity of forest canopies using large-eddy simulations. – Bound.-Layer Meteor. **132**, 351–382.

Brown, K., W. Covey, 1966: The energy-budget evaluation of the micro-meteorological transfer process within a cornfield. – Agric. Meteorol **3**, 73–96.

Cassiani, M., G. Katul, J. Albertson, 2008: The effects of canopy leaf area index on airflow across forest edges: large-eddy simulation and analytical results. – Bound.-Layer Meteor. **126**, 433–460.

Deardorff, J., 1980: Stratocumulus-capped mixed layers derived from a three-dimensional model. – Bound.-Layer Meteor. **18**, 495–527.

Dupont, S., Y. Brunet, 2008: Edge flow and canopy structure: a large-eddy simulation study. – Bound.-Layer Meteor. **126**, 51–71.

Dupont, S., Y. Brunet, 2009: Coherent structures in canopy edge flow: a large-eddy simulation study. – J. Fluid Mech. **630**, 93–128.

Edburg, S., D. Stock, B. Lamb, E. Patton, 2012: The effect of the vertical source distribution on scalar statistics within and above a forest canopy. – Bound.-Layer Meteor. **142**, 365–382.

Finnigan, J., 1979: Turbulence in waving wheat. ii. structure of momentum transfer. – Bound.-Layer Meteor. **16**, 213–236.

Finnigan, J., 2000: Turbulence in plant canopies. – Annu. Rev. Fluid Mech. **32**, 519–571.

Finnigan, J., R. Shaw, E. Patton, 2009: Turbulence structure above a vegetation canopy. – J. Fluid Mech. **637**, 387–424.

Foken, T., 2008: Micrometeorology – Springer Berlin Heidelberg, pp. 306.

Garratt, J., 1990: The internal boundary layer - a review. – Bound.-Layer Meteor. **50**, 171–203.

Inagaki, A., M. Castillo, Y. Yamashita, M. Kanda, H. Takimoto, 2012: Large-eddy simulation of coherent flow structures within a cubical canopy. – Bound.-Layer Meteor. **142**, 207–222.

Irvine, M., B. Gardiner, M. Hill, 1997: The evolution of turbulence across a forest edge. – Bound.-Layer Meteor. **84**, 467–496.

Jegede, O., T. Foken, 1999: A study of the internal boundary layer due to a roughness change in neutral conditions observed during the linex field campaigns. – Theor. Appl. Climatol **62**, 31–41.

Kanda, M., M. Hino, 1994: Organized structures in developing turbulent flow within and above a plant canopy, using a large-eddy simulation. – Boundary-Layer Meteorol **68**, 237–257.

Katul, G., J. Albertson, 1998: An investigation of higher-order closure models for a forested canopy. – Bound.-Layer Meteor. **89**, 47–74.

Katul, G., G. Kuhn, J. Schieldge, C. Hsieh, 1997: The ejection-sweep character of scalar fluxes in the unstable surface layer. – Bound.-Layer Meteor. **83**, 1–26.

Kruijt, B., W. Klaassen, R. Hutjes, 1995: Edge effects on diffusivity in the roughness layer over a forest. – In: Coutts, M., J. Grace (Eds.): Wind and Trees. – Cambridge University Press, Cambridge, 60–70.

Lenschow, D., J. Mann, L. Kristensen, 1994: How long is long enough when measuring fluxes and other turbulence statistics. – J. Atmos. Oceanic Technol. **11**, 661–673.

Letzel, M., S. Raasch, 2003: Large-eddy simulation of thermally induced oscillations in the convective boundary layer. – J. Atmos. Sci. **60**, 2328–2341.

Letzel, M., M. Krane, S. Raasch, 2008: High resolution urban large-eddy simulation studies from street canyon to neighbourhood scale. – Atmos. Env. **42**, 8770–8784.

Marshall, B., C. Wood, B. Gardiner, S. Belcher, 2002: Conditional sampling of forest canopy gusts. – Bound.-Layer Meteor. **102**, 225–251.

Monin, A., A. Obukhov, 1954: Osnovnye zakonomernosti turbulentnogo peremeshivanija v prizemnom sloe atmosfery (basic laws of turbulent mixing in the atmosphere near the ground). – Tr. Akad. Nauk SSSR Geophys. Inst. **24**, 163–187.

Morse, A., B. Gardiner, B. Marshall, 2002: Mechanisms controlling turbulence development across a forest edge. – Bound.-Layer Meteor. **103**, 227–251.

Patton, E., T. Horst, P. Sullivan, D. Lenschow, S. Oncley, W. Brown, S. Burns, A. Guenther, A. Held, T. Karl, S. Mayor, L. Rizzo, S. Spuler, J. Sun, A. Turnipseed, E. Allwine, S. Edburg, B. Lamb, R. Avissar, R. Calhoun, J. Kleissl, W. Massman, K. T. Paw U, J. Weil, 2011: The canopy horizontal array turbulence study. – Bull. Amer. Meteor. Soc. **92**, 593–611.

Raasch, S., D. Etling, 1998: Modeling deep ocean convection: large-eddy simulation in comparison with laboratory experiments. – J. Phys. Ocean. **28**, 1786–1802.

Raasch, S., T. Franke, 2011: Structure and formation of dust-devil-like vortices in the atmospheric boundary layer - a high resolution numerical study. – J. Geophys. Res. **116**, D16120.

Raasch, S., M. Schröter, 2001: Palm - a large-eddy simulation model performing on massively parallel computer. – Meteorol. Z. **10**, 363–372.

Raupach, M., 1981: Conditional statistics of Reynolds stress in rough-wall and smooth-wall turbulent boundary layers. – J. Fluid Mech. **108**, 363–382.

Raupach, M., J. Finnigan, Y. Brunet, 1996: Coherent eddies and turbulence in vegetation canopies: the mixing-layer analogy. – Bound.-Layer Meteor. **78**, 351–382.

Raynor, G., 1971: Wind and temperature structure in a coniferous forest and a contiguous field. – Forest Sci. **17**, 351–363.

Ruck, B., 1987: Laser doppler anemometry - a non-intrusive optical measuring technique for fluid velocity. – Part. Part. Syst. Charact. **4**, 26–37.

Ruck, B., E. Adams, 1991: Fluid mechanical aspects in the polutants transport to coniferous trees. – Bound.-Layer Meteor. **56**, 163–195.

Schröttle, J., A. Dörnbrack, 2013: Turbulence structure in a diabatically heated forest canopy composed of fractal pythagoras trees. – Theor. Comput. Fluid Dynam. **27**, 337–359.

Shaw, R., U. Schumann, 1992: Large-eddy simulation of turbulent flow above and within a forest. – Bound.-Layer Meteor. **61**, 47–64.

Shaw, R., G. D. Hartog, H. Neumann, 1988: Influence of foliar density and thermal stability on profiles of reynolds stress and turbulence intensity in a deciduous forest. – Bound.-Layer Meteor. **45**, 391–409.

Shir, C., 1972: A numerical computation of airflow over a sudden change of surface roughness. – J. Atmos. Sci. **29**, 304–310.

Stawiarski, C., K. Träumner, C. Knigge, R. Calhoun, 2013: Scopes and challenges of dual-doppler lidar wind measurements - an error analysis. – J. Atmos. Ocean. Tech. **30**, 2044–2061.

Steinfeld, G., M. Letzel, S. Raasch, M. Kanda, A. Inagaki, 2007: Spatial representativeness of single tower measurements and the imbalance problem with eddy-covariance fluxes: results of a large-eddy simulation study. – Bound.-Layer Meteor. **123**, 78–98.

Steinfeld, G., S. Raasch, T. Markkanen, 2008: Footprints in homogeneously and heterogeneously driven boundary layers derived from a lagrangian stochastic particle model embed-

ded into large-eddy simulation. – Bound.-Layer Meteor. **129**, 225–248.

Su, H., R. Shaw, K. T. Paw U, C. Moeng, P. Sullivan, 1998: Turbulent statistics of neutrally stratified flow within and above a sparse forest from large-eddy simulation and field observations. – Bound.-Layer Meteor. **88**, 363–397.

Su, H., R. Shaw, K. T. Paw U, 2000: Two-point correlation analysis of neutrally stratified flow within and above forest from large-eddy simulation. – Bound.-Layer Meteor. **49**, 423–460.

Sühring, M., S. Raasch, 2013: Heterogeneity-induced heat-flux patterns in the convective boundary layer: can they be detected from observations and is there a blending height? – a large-eddy simulation study for the litfass-2003 experiment. – Bound.-Layer Meteor. **148**, 309–338.

Sullivan, P., C. Moeng, B. Stevens, D. Lenschow, S. Mayor, 1998: Structure of the entrainment zone capping the convective atmospheric boundary layer. – J. Atmos. Sci. **55**, 3042–3064.

Thomas, C., J. Mayer, F. Meixner, T. Foken, 2006: Analysis of low-frequency turbulence above tall vegetation using doppler sodar. – Bound.-Layer Meteor. **119**, 563–587.

Tischmacher, M., B. Ruck, 2013: Interaction of gusts and forest edges - an experimental wind-tunnel study. – Forestry **86**, 523–532.

Träumner, K., C. Kottmeier, U. Corsmeier, A. Wieser, 2011: Convective boundary-layer entrainment: Short review and progress using doppler lidar. – Bound.-Layer Meteor. **141**, 369–391.

Träumner, K., A. Wieser, B. Ruck, C. Frank, L. Röhner, C. Kottmeier, 2012: The suitability of doppler lidar for characterizing the wind field above forest edges. – Forestry **85**, 399–412.

Wallace, J., H. Eckelmann, R. Brodkey, 1972: The wall region in turbulent flow. – J. Fluid Mech. **54**, 39–48.

Watanabe, T., 2004: Large-eddy simulation of coherent turbulence structures associated with scalar ramps over plant canopies. – Bound.-Layer Meteor. **112**, 307–341.

Wicker, L., W. Skamarock, 2002: Time-splitting methods for elastic models using forward time schemes. – Mon. Wea. Rev. **130**, 2088–2097.

Williamson, J., 1980: Low-storage runge-kutta schemes. – J. Comp. Phys. **35**, 48–56.

Yang, B., M. Raupach, R. Shaw, K. T. Paw U, A. Morse, 2006a: Large-eddy simulation of turbulent flow across a forest edge. part i: flow statistics. – Bound.-Layer Meteor. **120**, 377–412.

Yang, B., A. Morse, R. Shaw, K. T. Paw U, 2006b: Large-eddy simulation of turbulent flow across a forest edge. part ii: momentum and turbulent kinetic energy budgets. – Bound.-Layer Meteor. **121**, 433–457.

Zhu, J., X. Li, Y. Gonda, T. Matsuzaki, 2004: Wind profiles in and over trees. – J. Forestry Res. **15**, 305–312.